Proc. Natl. Acad. Sci. USA
Vol. 94, pp. 3448–3453, April 1997
Plant Biology

Voltage-dependent gating characteristics of the K^+ channel KAT1 depend on the N and C termini

IRENE MARTEN AND TOSHINORI HOSHI*

Department of Physiology and Biophysics, University of Iowa College of Medicine, Bowen Science Building 5-452, Iowa City, IA 52242

Communicated by Yuh Nung Jan, University of California School of Medicine, San Francisco, CA, January 22, 1997 (received for review October 16, 1996)

ABSTRACT **We studied how the C and N termini of the plant K^+ channel KAT1 influence the voltage-dependent gating behavior by generating C- and N-terminal deletion mutants. Functional expression was observed only when C-terminal deletions were downstream of the putative cyclic nucleotide binding site. Treatments of oocytes expressing KAT1 channels with anticytoskeletal agents indicated that intact microtubules are important for functional expression. C-terminal deletions altered the voltage sensitivity of the KAT1 channel with greater deletions resulting in smaller equivalent charge movements. In contrast, a deletion in the N terminus (Δ20–34) shifted the half-activation voltage by approximately −65 mV without markedly affecting the number of equivalent charges. The results reveal novel roles of the N and C termini in regulation of the voltage-dependent gating of KAT1.**

The cloned plant potassium channels, KAT1, AKT1/3, and KST1, functionally expressed in heterologous expression systems conduct inward currents upon hyperpolarization (1–7). Their amino acid sequences, however, are similar to those of the members of the *Shaker* superfamily such as the *Drosophila eag* channel, the human-related *eag* channel HERG and the cyclic nucleotide-gated (CNG) channel (5, 6, 8, 9; for review, see ref. 10). The structural organization of the KAT1 channel consists of six putative membrane-spanning domains (S1–S6) with a putative voltage-sensing S4 segment and a P-region between S5 and S6. The N and C termini are likely to face the cytoplasm and thus are accessible by intracellular regulatory factors (4).

Recent studies have shown that the members of the *Shaker* superfamily contain several definable functional domains. For example, the S4 and the S4–S5 linker segments appear to have major roles in voltage-sensing and activation (for review, see ref. 11). Some mutations in the S4 segment alter the equivalent charge movements associated with voltage-dependent activation (12). In contrast, the N-terminal domain is known to be important in N-type inactivation (13–15) and subunit assembly (16) while the C-terminal domain often contains regulatory-factor binding domains as in Ca^{2+}-dependent K^+ channels (*Slo*) (17) and CNG channels (18). The KAT1 channel subunit has a short N terminus with one potential phosphorylation site and a long C terminus with several putative regulatory sites (Fig. 1). The sequence similarity between a region of the KAT1 C terminus and the cAMP-binding domain of the *Escherichia coli* catabolite gene activator protein (20) suggests the presence of a cyclic nucleotide binding site in KAT1. Further, the KAT1 C terminus is rich in potential phosphorylation sites mediated by cAMP/cGMP-dependent protein kinases, Ca^{2+} calmodulin-dependent kinase II or protein kinase C (19), and putative protonation sites (e.g., histidines). The KAT1 homologs AKT1, AKT2, and AKT3 contain an ankyrin repeat domain in the C-terminal region, indicating a potential cytoskeletal binding segment (6, 9, 21). BLAST sequence comparison of the KAT1 C-terminal region with other proteins stored at the National Center for Biotechnology Information did not reveal a putative ankyrin-binding site but a potential microtubule-interaction site in the distal segment of the C terminus (position 563–631). This region is characterized by a highly basic profile (Fig. 1*A*) and shares an identity of ≈25% with a domain of the microtubule-associated proteins MAP1b (GenBank accession no. P14873), which enables the interaction between MAP1b and microtubules (22).

The KAT1 channel activity depends on membrane voltage as well as on extra- and intracellular modulatory factors. Hedrich *et al.* (3) and Hoshi (4) showed that acidification of the extra- or intracellular media shifts the voltage range of KAT1 activation toward more positive voltages. In addition, KAT1 gating is modulated by nucleotides and other yet unidentified intracellular factors as suggested by (*i*) the rundown in channel activity through patch excision, (*ii*) the ATP-induced maintenance/recovery of the channel activity in excised membrane patches, and (*iii*) the cGMP-induced shift of the current–voltage (*I–V*) curve to more negative voltages (4). Using mutagenesis, electrophysiological, and pharmacological approaches, we examined how the C- and N-terminal segments contribute to the KAT1 channel gating. Our results show that the N- and C-terminal domains have novel roles in regulating the voltage-dependent gating behavior, previously thought to be mediated largely by the core putative transmembrane segments.

MATERIALS AND METHODS

Molecular Biology. N- and C-terminal deletions of KAT1 were generated by PCR cassette mutagenesis and sequences of the PCR-amplified segments were verified by the DNA core facility of the University of Iowa. The LASERGENE NAVIGATOR program (DNAstar, Madison, WI) was used to analyze DNA and protein sequences. The oocytes were prepared and injected with RNAs essentially as described by Hoshi (4).

Electrophysiology. Whole-oocyte and macropatch recordings were performed essentially as described by Avdonin *et al.* (23). The analysis of the deactivation kinetics and determination of the conductance–voltage (*G–V*) curves were performed without leak subtraction. The *G–V* curves were calculated upon the tail current amplitude recorded at a constant deactivating voltage pulse after a series of hyper- and depolarizing voltage pulses. In most experiments, the tail currents were recorded at −50, −60, or −70 mV. For the measurement on the Δ501–677 channel in the presence of 20 mM KCl (see

The publication costs of this article were defrayed in part by page charge payment. This article must therefore be hereby marked "*advertisement*" in accordance with 18 U.S.C. §1734 solely to indicate this fact.

0027-8424/97/943448-6$2.00/0
PNAS is available online at **http://www.pnas.org**.

Abbreviations: CNG, cyclic nucleotide-gated; *G–V*, conductance–voltage; *I–V*, current–voltage.

*To whom reprint requests should be addressed. e-mail: Toshinori-Hoshi@uiowa.edu.

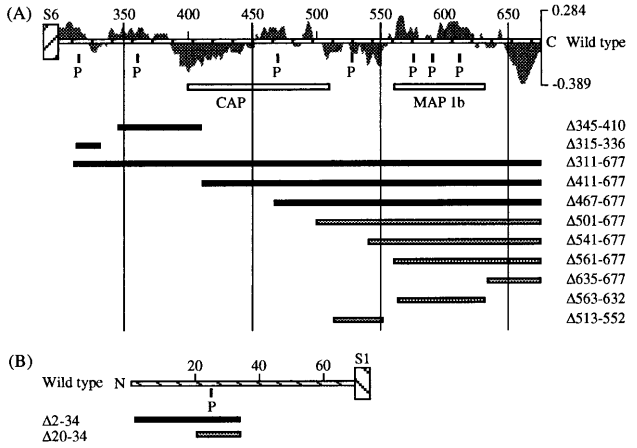

FIG. 1. Effects of C- and N-terminal deletions on functional expression of KAT1. Schematic representation of the KAT1 C (*A*) and N (*B*) termini (striped horizontal bars) and their putative regulatory sites [p, protein phosphorylation sites according to Pearson and Kemp (19); CAP, cyclic nucleotide binding site; MAP1b, microtubule-associated protein interaction site; CAP/MAP1b, open bars). The average charge of the C terminus calculated by summing the charges over a range of 18 residues at pH 7.2 is illustrated as shaded areas underlying the striped horizontal bar in *A*. Deleted regions are given by black and gray horizontal bars indicating nonfunctional or functional expression of the appropriate channel mutant, respectively.

Fig. 5*A*), and on the Δ20–34 channel, the tail currents were determined at 30 mV and −80 mV, respectively. The macroscopic conductance data points were fitted with a simple Boltzmann distribution as given by the following function: $G(V) = 1/\{1 + \exp[-(V - V_{1/2})zF/RT]\}$ where R, T, and F have the usual meanings, z represents the number of equivalent charges, and $V_{1/2}$ is the half-activation voltage where 50% of the maximal conductance level is reached. If not otherwise mentioned, results are presented as mean ± SD (n = number of experiments). Error bars in figures represent SD.

Solutions. Two-electrode voltage-clamp experiments were performed in the presence of 50 mM KCl, 90 mM NaCl, 2 mM $MgCl_2$, and 10 mM Hepes (pH 7.2). The standard extracellular patch-clamp solution contained 140 mM KCl, 2 mM $MgCl_2$, and 10 mM Hepes (pH 7.2) while the standard internal/bath patch-clamp solution was composed of 140 mM KCl, 2 mM $MgCl_2$, 11 mM EGTA, and 10 mM Hepes (pH 7.2). The patch-clamp experiments at a low intracellular pH were performed in 140 mM KCl, 2 mM $MgCl_2$, 11 mM EGTA, and 10 mM Mes (pH 6.2). The pH of the solutions was adjusted with *N*-methyl-D-glucamine. Other solutions used are mentioned in the figure legends. Cytochalasin-D (Sigma) and nocodazole (Calbiochem) were dissolved in dimethyl sulfoxide (DMSO, cytochalasin-D: 1 mg/ml; nocodazole: 1.5 mg/ml) whereas colchicine (Sigma) was dissolved in ethanol (EtOH, 40 mg/ml). Drug-containing ND96 solutions were prepared fresh by adding sufficient stock to obtain a final concentration of 20 μM cytochalasin-D/1% DMSO, 50 μM nocodazole/1% DMSO, or 100 μM colchicine/0.1% EtOH. Control ND96 solutions were prepared by adjusting the final vehicle concentrations (EtOH or DMSO) to 0.1% or 1% (vol/vol), respectively. To prevent photodestruction of the drugs, the oocytes were treated with agent-containing or agent-free ND96 solutions in the dark.

RESULTS

Cytoskeletal Elements Do Not Control the Voltage-Dependent Gating Behavior of KAT1. We first examined whether the rundown of the KAT1 activity observed on patch excision was caused by a loss of interaction between the channel protein and cytoskeleton. This hypothesis predicts that treatments with cytoskeleton-disrupting agents mimic the rundown process by changing the kinetics or shifting the macroscopic *G–V* curve to more negative voltages (4). Two days after injection of KAT1 RNA, we incubated the oocytes in 100 μM colchicine, a microtubule disrupter (24). After more than 21 h, the electrical properties of the oocytes were studied with the two-electrode voltage-clamp technique. Hyperpolarizing pulses to more negative than −80 mV elicited time-dependent inward currents in both control and colchicine-treated cells, and the currents declined instantaneously upon depolarization (Fig. 2*A*). Though other interpretations are possible (25, 26), the terminology "activation" and "deactivation" is used throughout this work to describe the hyperpolarization-induced rise and repolarization-dependent decay in the current amplitude, respectively. The colchicine-treatment reduced the mean current amplitude at −120 mV measured from the same batch of oocytes by 47% (Fig. 2*A*). Using tail current amplitudes, *G–V* curves were determined for both experimental conditions and fitted with a simple Boltzmann function (Fig. 2*A*). Colchicine altered neither the midpoint voltage of activation ($V_{1/2} \approx -111$ mV) nor the number of equivalent charges ($z \approx 1.6$; Fig. 2*B*). The colchicine treatment did not affect the kinetics of the KAT1 channel. Neither the deactivation time constant (τ) nor the half-activation time ($t_{1/2}$) were altered (Fig. 2 *C* and *D*). When colchicine was extracellularly applied to KAT1-expressing oocytes, an immediate decline in the current amplitude was not observed. In addition to colchicine, the drug nocodazole (24) and/or low temperature, both which are known to disrupt the microtubule integrity, also affected the KAT1 current amplitude. Preincubation of oocytes at 8°C (4 h) followed by nocodazole treatment (50 μM, >12 h at 17°C) reduced the steady-state current amplitude by 74.6% in a statistical significant manner [two-sample t test: $P = 0.0011$; $I_{\text{nocodazole}} = -1.6 \pm 0.2$ μA (SEM), $n = 16$; $I_{\text{control}} = -6.3 \pm 1.1$ μA (SEM), $n = 16$]. Low temperature (8°C for 4–6 h) decreased the amplitude by 37.3%, but the effect was not statistically significant ($P = 0.1521$; $I_{8°C} = -4.2 \pm 0.7$ μA (SEM), $n_{8°C} = 16$; $I_{17°C} = -6.7 \pm 1.1$ μA (SEM), $n_{17°C} = 14$). The action of the antiactin agent cytochalasin-D was also studied (27). After treatment of KAT1-expressing oocytes with 20 μM cytochalasin-D for at least 13 h, the *G–V* curves obtained from control and cytochalasin-treated cells were not markedly different (Fig. 2*E*). But unlike colchicine, cytochalasin-D did not decrease the mean steady-state current amplitude (Fig. 2*F*). Similar results were obtained when treatment with cytochalasin-D was done for at least 23 h (data not shown). Both anticytoskeletal agents, colchicine and cytochalasin-D, failed to shift the *G–V* curve or to slow down the activation kinetics. Although microtubules are not solely responsible for the channel rundown, they are important for functional expression of the wild-type KAT1 channel.

If the putative microtubule-binding site in the C terminus is involved in KAT1 rundown, deletion of the motif should result in nonfunctional expression and eliminate the colchicine sensitivity. Thus, we constructed a deletion mutant (Δ563–632) which lacked the cytoskeletal binding motif (Fig. 1*A*). The representative current traces and the *G–V* curves determined from the same batch of oocytes indicate that the deletion neither prevented functional expression nor altered the voltage-dependent properties of KAT1 (Fig. 3 *A* and *B*). The measured half-activation voltages for the wild-type and the Δ563–632 channel were −111.7 ± 1.6 mV ($n = 5$) and −116.0 ± 5.6 mV ($n = 6$), and the equivalent charges were 1.66 ± 0.14 ($n = 5$) and 1.56 ± 0.15 ($n = 6$), respectively (Fig. 3*B*). We further incubated oocytes expressing the Δ563–632 channels for 22–30 h in 100 μM colchicine. The colchicine treatment decreased the current amplitude at −120 mV by 43% (Fig. 3*C*). This fractional reduction was similar to the

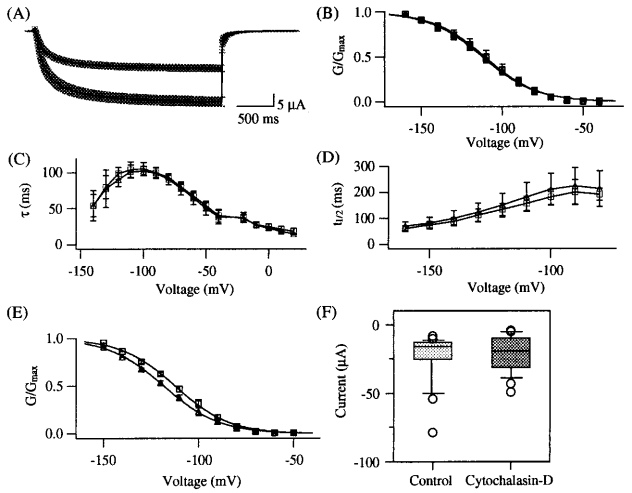

FIG. 2. Effects of anticytoskeletal agents on KAT1. (*A*) The average currents induced by a voltage step from −10 to −120 mV in oocytes from the same batch were recorded after exposure to colchicine-containing (100 μM colchicine, upper trace, $n = 12$) or colchicine-free ND96 solution (lower trace, $n = 10$) for at least 21 h at 17°C. Solid black lines represent the mean current amplitude, the shaded areas show the corresponding SEM. (*B*) No change in KAT1 voltage dependence after colchicine treatment. Normalized *G–V* curves for KAT1 obtained from tail current measurements at −50 mV were fitted with a simple Boltzmann distribution (Δ control: $V_{1/2\,\Delta} = -112.1 \pm 3.2$ mV, $z_\Delta = 1.53 \pm 0.14$, $n_\Delta = 8$; □ colchicine, $V_{1/2\,\square} = -110.8 \pm 5.7$ mV, $z_\square = 1.57 \pm 0.14$, $n_\square = 8$). (*C*) No effect of colchicine on KAT1 deactivation kinetics. Following a constant hyperpolarizing voltage step to activate the KAT1 channels, tail currents were recorded at different voltages (−140 to 20 mV in 10-mV increments). Time course of the current decline was fitted with the sum of two exponential functions. The fast deactivation time constants are plotted against the voltage ($n_\Delta = 7$–8, $n_\square = 6$–9, depending on the voltage). (*D*) No effect of colchicine on KAT1 activation kinetics. The half-activation time $t_{1/2}$ is given as a function of voltage. It represents the time at which the half-maximal current amplitude evoked by a 2.5-s voltage pulse is reached ($n_\Delta = 8$–17, $n_\square = 9$–14, depending on the voltage). Symbols used in *C* and *D* have the same meaning as in *B*. (*E*) No change in KAT1 voltage dependence after cytochalasin-D treatment. Normalized *G–V* curves for KAT1 wild type were determined from tail current measurements using the same batch of oocytes at −60 mV after incubation in drug-containing (20 μM cytochalasin-D □; $V_{1/2} = -112.1 \pm 6.0$ mV, $z = 1.81 \pm 0.08$, $n = 4$) or drug-free ND96 solution (Δ; $V_{1/2} = -118.0 \pm 1.7$ mV, $z = 1.72 \pm 0.13$, $n = 6$) for at least 13 h at 17°C. (*F*) Box plots of the maximal current amplitude elicited at −140 mV in oocytes treated as described in *E* ($n_{\text{control}} = 25$; $n_{\text{cytochalasin-D}} = 18$).

reduction observed in colchicine-treated oocytes expressing KAT1 wild type (Fig. 2*A*). If loss of interaction through the putative cytoskeletal interaction domain deleted in the Δ563–632 channel is responsible for the rundown, properties of the Δ563–632 channel after patch excision are expected to be different from those of the wild-type channel. However, as with the wild-type channel, the Δ563–632 channel underwent the rundown process on patch excision. Fig. 3*D* shows that the *I–V* curves shifted to more negative voltages after the inside-out configuration was established. As reported for the wild-type KAT1 channel (4), rundown of the Δ563–632 channel was also accompanied by a slow-down in the activation time course (data not shown). Thus, neither the colchicine effect nor the rundown is mediated by the C-terminal region 563–632 of KAT1.

The Putative Cyclic Nucleotide Binding Domain Is Important for Functional Expression of KAT1. In addition to the deletion Δ563–632, we made other deletions in the carboxyl segment to identify amino acid residues involved in regulation of KAT1 gating (Fig. 1*A*). Functional expression of mutant channels was tested with both hyper- and depolarizing voltage pulses (Figs. 3*A* and 4*A*). Hyperpolarization-induced K^+ currents were not detected over a broad voltage range (−180 to 10 mV) from channel mutants containing deletions in the putative cyclic nucleotide binding domain or in the segment between S6 and this cyclic nucleotide binding domain (Δ345–410, Δ315–336, Δ311–677, Δ411–677, Δ467–677; Fig. 1*A*, black horizontal bars). Pulses to very negative voltages (e.g., −180 mV) frequently elicited only endogenous inward currents as described by Tzounopoulos *et al.* (28). In contrast, when deletions were made downstream of the cyclic nucleotide binding domain, hyperpolarization-induced inward K^+ currents were observed as shown for the channel mutants Δ563–632 and Δ501–677 in Figs. 3*A* and 4*A*, respectively. The results show that the putative cyclic nucleotide binding domain is required for functional expression of KAT1.

Based on the deletion results described above, we hypothesized that proteolytic cleavage of the C-terminal domain should convert a functional into a nonfunctional KAT1 channel. We inserted four additional amino acid residues (Ile-Glu-Gly-Arg) at position 310, representing the cleavage site of the restriction protease factor Xa. Unfortunately, the insertion itself caused nonfunctional expression of the mutant channel, preventing us from testing the effects of the C-terminal backbone cleavage by factor Xa.

We further examined whether the distal segment of the C terminus contributes to the modulatory phenomena of the wild-type channel, such as rundown behavior and intracellular pH sensitivity (4). Recordings from the Δ501–677 channel were performed using the macropatch-clamp method. We found that the Δ501–677 channel activity still underwent rundown on patch excision, and that a change of the intracellular pH from 7.2 to 6.2 resulted in a shift of the *I–V* curve to more positive voltages as shown for the wild-type channel (data not shown). Since the putative cyclic nucleotide binding site is still present in the Δ501–677 channel, the sensitivity of this mutant channel toward intracellular cGMP is very likely maintained and therefore, was not tested. Thus, the distal segment of the C terminus does not mediate rundown behavior and is not required for the intracellular pH sensitivity of the KAT1 channel.

C-Terminal Deletions Influence the Voltage Sensitivity of KAT1. Voltage sensitivity of a channel can be inferred from the equivalent charge movement associated with its *G–V* curve while both voltage-dependent and -independent gating tran-

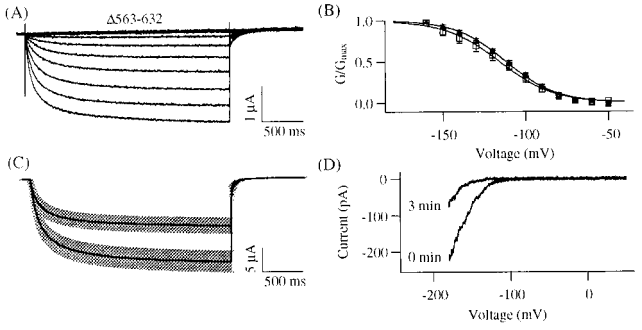

FIG. 3. Properties of the Δ563–632 channel. (*A*) Representative current traces evoked in response to 2.5-s voltage pulses from −150 to −30 mV in 10-mV increments from a holding voltage of −10 mV. Tail currents were recorded at −60 mV. (*B*) Normalized *G–V* curves for KAT1 wild type (Δ, $n = 5$) and Δ563–632 channel (□, $n = 6$). (*C*) Comparison of the mean current amplitudes at −120 mV measured from the oocytes treated with colchicine-free ND96 solution (lower solid black line, $n = 17$) or with 100 μM colchicine-containing ND96 solution (upper solid black line, $n = 18$) for >22 h at 17°C. The shaded regions represent the corresponding SEM. (*D*) Current-voltage curves obtained by 2-s ramps from 50 to −190 mV were recorded in the inside-out configuration immediately (0 min) and 3 min after patch excision.

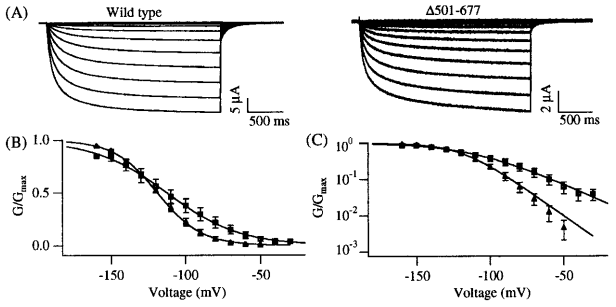

FIG. 4. Decrease in the charge movement of the Δ501–677 channel. (*A*) Representative current traces of KAT1 wild-type (*Left*) and the channel mutant Δ501–677 (*Right*) elicited in response to voltage pulses from −150 mV to −30 mV in 10-mV increments from a holding voltage of −10 mV. The Δ501–677 currents were recorded in the presence of 50 mM KCl, 90 mM NaCl, 2 mM $MgCl_2$, 0.5 mM $CaCl_2$, and 10 mM Hepes (pH 7.2). (*B*) Linear plot of normalized *G–V* curves determined for KAT1 wild-type (Δ, $n = 5$) and the Δ501–677 channel (□, $n = 7$) from the same batch of oocytes. The extracellular solution contained 20 mM KCl, 120 mM NaCl, 2 mM $MgCl_2$, 10 mM Hepes (pH 7.2). (*C*) Semilogarithmic plot of the *G–V* curves shown in *B*. Similar half-activation voltages and equivalent gating charges were estimated for the Δ501–677 channel in the presence of different extracellular K^+ concentrations (20 mM K^+ in *B* and *C* vs. 50 mM K^+ in Fig. 5 *A* and *B*).

sitions contribute to the half-activation voltage. We found that C-terminal deletions altered the voltage sensitivity of the KAT1 channel in a systematic way. *G–V* curves from tail currents were measured for each functional channel mutant (Figs. 3*A* and 4*A*). In Fig. 4 *B* and *C*, the *G–V* curves for the wild-type and Δ501–677 channels measured from the same batch of oocytes were plotted on linear and semilogarithmic axes. This deletion did not noticeably affect the half-activation voltage ($V_{1/2\ \text{wild type}} = -118.9 \pm 1.9$ mV, $n = 5$; $V_{1/2\ \Delta501-677} = -112.5 \pm 9.9$ mV, $n = 7$, two-sample *t* test: $P = 0.5562$; Fig. 4 *B* and *C*). However, the *G–V* curve from the Δ501–607 channel was markedly less steep than that from the wild-type KAT1 channel. The number of equivalent charges estimated for the Δ501–677 channel was $z_{\Delta501-677} = 1.05 \pm 0.08$ ($n = 7$), about 39% lower than the number obtained for the wild-type channel ($z_{\text{wild type}} = 1.71 \pm 0.17$, $n = 5$). This difference was statistically significant (two-sample *t* test, $P = 0.0043$). The limiting slope measurements (29) were not possible because the very small tail current amplitudes at depolarizing potentials prevented reliable calculations of the required $G/G_{\max}$ values ($\ll 0.001$) at voltages where the open probability is very small.

The half-activation voltages and the number of equivalent charges determined for KAT1 wild type and all functional C-terminal deletion mutants are summarized in Fig. 5 *A* and *B*. The results show that the number of equivalent charges decreases with the increasing number of amino acids truncated from the C terminus (Fig. 5*B*) with a high linear correlation coefficient ($R = -0.907$). Since a change in the net charge of the C terminus did not alter the voltage sensitivity in a predictable manner ($R = -0.287$, Fig. 5*C*), the overall net charge of the C terminus seems not to be important for the voltage-sensing process. However, there was a high correlation between the number of equivalent charges and the number of either positively or negatively charged residues removed from the C terminus (Fig. 5*D*, $R = -0.873$ for deleted positive charges, and Fig. 5*E*, $R = -0.893$ for deleted negative charges). The results suggest that the distal segment of the C terminus influences the voltage-sensing mechanism of the KAT1 channel in a graded manner.

In contrast, the C-terminal deletions did not systematically affect the half-activation voltage (Fig. 5*A*). While a shift in the half-activation voltage of about 12 mV along the voltage axis was found for the Δ541–677 channel ($V_{1/2\ \Delta541-677} = -129.0 \pm 4.6$ mV, $n = 4$; $V_{1/2\ \text{wild type}} = -116.3 \pm 1.6$ mV, $n = 6$), and the Δ513–552 channel ($V_{1/2\ \Delta513-552} = -105.6 \pm 3.0$ mV, $n = 9$; $V_{1/2\ \text{wild type}} = -117.2 \pm 2.0$ mV, $n = 3$), the half-activation voltage of KAT1 was not markedly altered by other deletions.

To elucidate whether the decrease in the overall charge movement is linked to the charge movement (z_C) associated with the closing transition, the voltage dependence of the deactivation time course of Δ501–677 was studied by measuring tail currents at voltages where the steady-state open-channel probability is negligible (Fig. 6*A*; see Fig. 4 *A* and *B*). Tail currents were fitted with single exponentials and their time constants were plotted in Fig. 6*B*. At the voltages recorded, the deactivation time course of the Δ501–677 channel was slower than that of the wild-type channel. The voltage dependence of the relaxation time constant of the wild-type and the Δ501–677 channels corresponds to a charge movement of $z_{C\ \text{wild type}} = 0.55$ and $z_{C\ \Delta501-677} = 0.28$, respectively. Thus, the reduced voltage dependence of the closing transition is in part responsible for the decrease in the voltage dependence of the steady-state macroscopic conductance.

The N-Terminal Deletion Δ20–34 Alters the Half-Activation Voltage of KAT1. The short N terminus of KAT1 contains one putative cGMP-dependent phosphorylation site (19). We examined whether the N terminus might be involved in modulation and/or determination of voltage-dependent gating characteristics of KAT1. When half of the N terminus (Δ2–34, Fig. 1*B*) was removed, macroscopic K^+-selective inward currents were not detected in response to large hyperpolarizing pulses (e.g. −180 mV, data not shown). A shorter deletion, Δ20–34

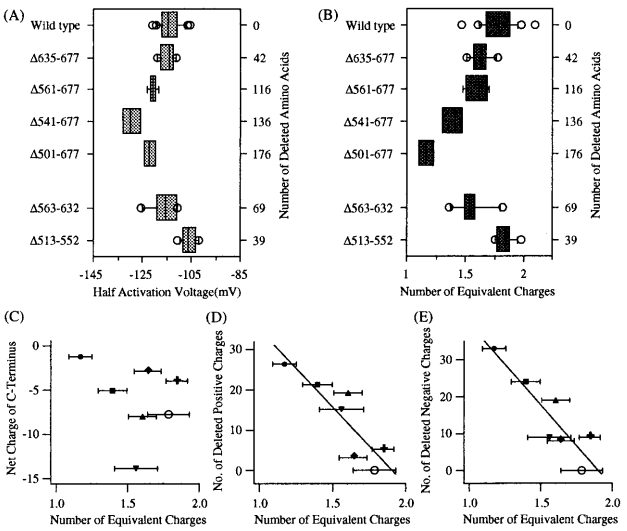

FIG. 5. Voltage dependence of the C-terminal deletion mutant channels. Box plots of the half-activation voltage (*A*) and the number of equivalent charges associated with steady-state activation (*B*) are shown for KAT1 wild-type and the functional C-terminal deletion mutants ($n_{\text{wild type}} = 20$; $n_{\Delta635-677} = 6$; $n_{\Delta561-677} = 5$; $n_{\Delta541-677} = 4$; $n_{\Delta501-677} = 4$; $n_{\Delta563-632} = 6$; $n_{\Delta513-532} = 9$). The two-electrode voltage-clamp measurements for the Δ501–677 channel in *A* and *B* were performed with additional 0.5 mM $CaCl_2$ in the extracellular solution. (*C–E*) The mean of the number of equivalent charges calculated for the wild-type channel (open circle) and the mutant channels were plotted against the corresponding net charge remaining in the entire C-terminal domain (*C*) or against the corresponding number of positively (*D*) or negatively (*E*) charged amino acids removed from the C terminus. Data points were analyzed with a simple linear regression (solid lines) with $R = -0.907$ in *B*, $R = -0.287$ in *C*, $R = -0.873$ in *D*, and $R = -0.893$ in *E*. Symbols have following meanings: the Δ513–552 channel, +; the Δ635–677 channel, ◆; the Δ563–632 channel, ▼; the Δ561–677 channel, ▲; the Δ541–677 channel, ■; the Δ501–677 channel, ●.

(Fig. 1*B*), however, produced functional channels, and the representative current traces are shown in Fig. 7*A*. This short N-terminal deletion markedly altered the voltage dependence of the steady-state activation. The tail current *G–V* curve of Δ20–34 (Fig. 7*B*) shows a shift in the half-activation voltage of about 65 mV toward more negative voltages ($V_{1/2\ \Delta 20-34} = -169.2 \pm 8.2$ mV, $n = 3$; $V_{1/2\ \text{wild type}} = -104.1 \pm 2.4$ mV, $n = 3$). In contrast to some of the C-terminal deletions, the N-terminal deletion Δ20–34 did not affect the voltage sensitivity of the channel as indicated by the similar steepness of the *G–V* curves ($z_{\Delta 20-34} = 1.61 \pm 0.24$, $n = 3$; $z_{\text{wild type}} = 1.79 \pm 0.35$, $n = 3$). The change in the half-activation voltage is in part caused by the faster deactivation process in the Δ20–34 channel. Tail currents recorded from the wild-type and Δ20–34 channels at −120 mV and compared in Fig. 7*C* were fitted with the sum of two exponentials. The fast deactivation time constant determined for the wild-type channel and the Δ20–34 channel was $\tau = 103.0$ ms and $\tau = 35.7$ ms, respectively.

Despite the change in the half-activation voltage, the sensitivity toward intracellular regulatory factors are maintained in the Δ20–34 channel. Fig. 7*D* illustrates that the channel showed rundown on patch excision, with the *I–V* curve shifting to more negative voltages in the inside-out configuration. Accordingly, a voltage pulse to −200 mV did not induce inward currents (Fig. 7*E*, upper trace). However, when the intracellular pH was changed from 7.2 to 6.2, time-dependent inward currents were again recorded (Fig. 7*E*, lower trace). Thus, the residues 20–34 do not mediate the rundown or the pH sensitivity of KAT1.

DISCUSSION

We examined the roles of the N and C termini in regulation of the KAT1 channel gating. It was previously believed that the voltage-dependent gating properties of channel activation were primarily dependent on the transmembrane segments of the channel, such as the S4 segment. However, our results show that the N and the C termini of the KAT1 channel are extremely important in KAT1 channel function, playing crucial roles in voltage-dependent gating and in functional expression of the channel protein.

Microtubules Control KAT1 Expression. We hypothesized that the separation of KAT1 channels from the cytoskeletal network by patch excision is responsible for the rundown, characterized by a very large shift in the voltage dependence to a more negative direction (4). We tested this hypothesis by deleting the putative microtubule-interacting domain of KAT1 and by studying the effects of colchicine, nocodazole, and cytochalasin-D, known disrupters of microtubules and microfilaments (24, 27). None of these manipulations mimicked the changes in the gating properties associated with channel rundown (Fig. 2). The results suggest that the functional expression of KAT1 channel proteins depends on the integrity of microtubules.

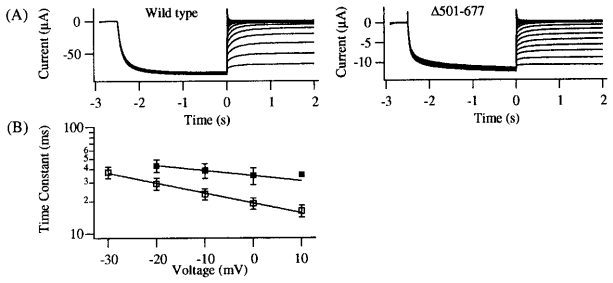

FIG. 6. Voltage dependence of the deactivation time course of the Δ501–677 channel. (*A*) Tail currents for KAT1 wild-type (*Left*) and the Δ501–677 channel (*Right*) were recorded at −130 to 30 mV for KAT1 wild-type or −140 to 30 mV for Δ501–677 following an activating pulse to −140 mV (wild type) or −150 mV (Δ501–677). (*B*) Tail currents derived as shown in *A* were fitted with a sum of two exponentials. The fast deactivation time constants are plotted against the voltage. Solid lines represent simple exponential fits of the voltage dependence of the time constants. (KAT1 wild type = □, $z_{C\ \square} = 0.55 \pm 0.06$, $n = 8$; Δ501–677 channel = ■, $z_{C\ \blacksquare} = 0.28 \pm 0.05$, $n = 2$).

Intracellular Modulation of Functional KAT1 Mutants. The sensitivity of the functional C- and N-terminal channel mutants toward intracellular factors are unaltered. They show rundown on patch excision, and they are regulated by the internal pH (Fig. 7*E*). Removal of four potential phosphorylation sites distal to the putative cyclic nucleotide binding domain and one in the N terminus (Fig. 1) did not alter rundown behavior. If rundown is related to the phosphorylation status, then other phosphorylation sites are more likely to be involved in channel modulation. Maintenance of the pH sensitivity and the rundown susceptibility in the channel mutants Δ501–677 and Δ20–34 indicates that the amino acid residues elsewhere are responsible for the modulatory phenomena.

C Terminus Determines Functional Expression of KAT1. C-terminal channel mutants with deletions in the segment between S6 and the putative cyclic nucleotide binding domain (inclusive) were electrophysiologically nonfunctional (Fig. 1*A*). Insertion of only four amino acid residues representing the consensus sequence of the restriction protease factor Xa directly behind the S6 segment also produced nonfunctional channels. Thus, the region between the S6 segment and the putative cyclic nucleotide binding site (residue 311–501) is crucial for functional expression of the KAT1 channel. However, we do not have direct evidence indicating whether the KAT1 subunits are not properly integrated into the plasma membrane or they are inserted but electrophysiologically nonfunctional. In the rod cyclic nucleotide-gated channel, a short 34-amino acid truncation of the C terminus disrupted the

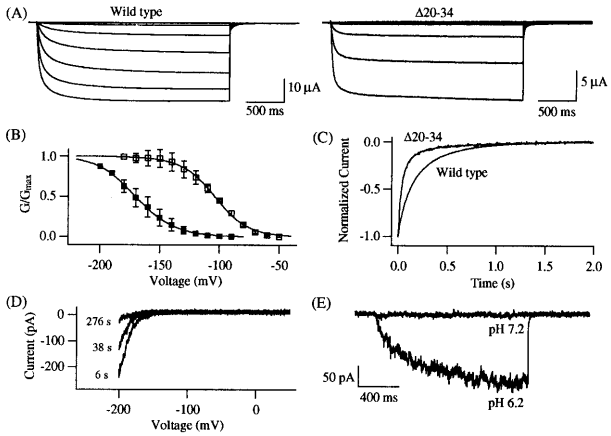

FIG. 7. Electrical properties of the Δ20–34 channel. (*A*) Inward-rectifying currents recorded from KAT1 wild type and the channel mutant Δ20–34 were elicited in response to voltage steps to −180 mV to −40 mV in 20-mV increments from a holding voltage of −10 mV. Tail currents were obtained at −50 mV (KAT1 wild type) or −80 mV (channel mutant Δ20–34). (*B*) Normalized *G–V* curves calculated for KAT1 wild-type (□, $n = 3$) and the Δ20–34 channel (■, $n = 3$). The composition of the bath solution in *A* and *B* was as follows: 50 mM KCl, 90 mM NaCl, 2 mM $MgCl_2$, 0.5 mM $CaCl_2$, and 10 mM Hepes (pH 7.2). (*C*) Deactivation of the Δ20–34 channel. The decline of normalized tail currents from wild-type and Δ20–34 channels evoked at −120 mV after an activating pulse to −150 mV (wild type) or −170 mV (Δ20–34) is shown. (*D*) *I–V* curves of the Δ20–34 channels were obtained by 1.5-s ramps from 50 to −200 mV and recorded in the inside-out configuration at different times after patch excision. (*E*) Effects of low internal pH on the mutant currents elicited by a voltage pulse to −200 mV from a holding voltage of 0 mV in the inside-out configuration of the same macropatch presented in *D*. The current traces were successively recorded at pH 7.2 and 6.2.

functional expression by preventing a proper integration into the plasma membrane (30). However, the truncation of the entire C terminus of a mouse *Shaker*-like K^+ channel destroyed the function rather than the assembly or integration of the protein into the plasma membrane (31).

The KAT1 C Terminus Contributes to the Voltage Sensor. In the *Shaker*-like channels, those mutations in the putative transmembrane segments have been shown to affect the voltage sensitivity (for review, see ref. 11). Mutations of the charged residues in the transmembrane S4 segment often alter the voltage sensitivity indicated by changes in the number of equivalent gating charges (12). However, we found that the deletion of a putative cytoplasmic C-terminal segment (Δ501–677) decreased the equivalent charge movement of the KAT1 channel by about 40% (Figs. 4 and 5). The decrease in the voltage sensitivity is highly correlated with the length of the truncated C-terminal region, with a greater deletion resulting in a smaller equivalent charge movement (Fig. 5*B*). Thus, the KAT1 C terminus has a novel role of contributing to or regulating the voltage sensor of the channel. The high linear correlation of the gating charge movement with the change in the number of positively and negatively charged residues rather than to the net charge of the entire C terminus (Fig. 5 *C–E*) supports the idea that the distal segment of the C terminus between 501–677 interacts with the voltage-sensing apparatus in a graded manner. The KAT1 C terminus could directly interact with the cytoplasmic end of the S4 segment (32) or with the amino acid residues that surround the S4 segment (33) to change the effective charge movement. It will be important to obtain physical evidence that the voltage sensor of the KAT1 channel, probably S4, interacts with the C-terminal domain.

The KAT1 N Terminus also Contributes to the Voltage-Dependent Gating. The removal of the residues 20–34 retained channel function and drastically affected the gating properties. The activation curve shifted to more negative voltages by 65 mV (Fig. 7*B*) by accelerating the deactivation time course. In contrast to the C-terminal deletions that changed the equivalent charge movement, the Δ20–34 deletion did not affect the voltage sensitivity. Thus, unlike the N termini of many *Shaker*-like channels, which are involved in N-type inactivation (13), the KAT1 channel N terminus regulates the deactivation gating property. Recently, similar effects of the N terminus on the voltage-dependent gating were found for HERG (34). Based on the shift of the *G–V* curve, removal of residues 20–34 destabilize the open channel by about 2 kcal/mol. This novel role of the KAT1 N terminus in control of the channel gating may be analogous to that of the N terminus of CNG channel, which appears to allosterically influence its C terminus to affect the cyclic nucleotide sensitivity (35). Considering that the Δ20–34 deletion shifts the activation curve to a more negative voltage, it is possible that the voltage dependence of the apparently nonfunctional Δ2–34 channel with a larger deletion may be shifted even more, beyond the voltage range tolerated by the oocytes, not allowing the recording of macroscopic K^+ currents.

The regulation mechanisms of the KAT1 channel through its C and N termini resemble those of the related CNG channels (35). The KAT1 and CNG channel activation are promoted by their N termini (Figs. 1*B* and 7; ref. 35). The functional expression of both KAT1 and CNG depends on their C termini (Fig. 1*A*; ref. 35). It will be interesting to investigate the roles of N and C termini in activation/deactivation gating in a variety of voltage-dependent channels. Since both the N- and C-terminal segments are likely to face the intracellular side, the phenomena described here may be involved in modulation of the voltage dependence of the channel by other channel subunits, enzymes and cytoskeletal elements.

We thank J. Kabat and M. Ciorba for technical assistance; D. J. Henniger for performing some early experiments; V. B. Avdonin, M. L. Chen, J. Kabat and X. D. Tang for critical comments on the manuscript; and J. Marshall for amplification. This work was supported in part by an Human Frontier Science Program fellowship to I.M. (LT380/95) and a National Institutes of Health grant to T. H. (GM51474). T.H. was also supported by Klingenstein Foundation and McKnight Endowment.

1. Schachtman, D. P., Schroeder, J. I., Lucas, W. J., Anderson, J. A. & Gaber, R. F. (1992) *Science* **258,** 1654–1658.
2. Bertl, A., Anderson, J. A., Slayman, C. L. & Gaber, R. F. (1995) *Proc. Natl. Acad. Sci. USA* **92,** 2701–2705.
3. Hedrich, R., Moran, O., Conti, F., Busch, H., Becker, D., Gambale, F., Dreyer, I., Kuech, A., Neuwinger, K. & Palme, K. (1995) *Eur. Biophys. J.* **24,** 107–115.
4. Hoshi, T. (1995) *J. Gen. Physiol.* **105,** 309–328.
5. Müller-Röber, B., Ellenberg, J., Provart, N., Willmitzer, L., Busch, H., Becker, D., Dietrich, P., Hoth, S. & Hedrich, R. (1995) *EMBO J.* **14,** 2409–2416.
6. Ketchum, K. A. & Slayman, C. W. (1996) *FEBS Lett.* **378,** 19–26.
7. Marten, I., Gaymard, F., Lemaillet, G., Thibaud, J. B., Sentenac, H. & Hedrich, R. (1996) *FEBS Lett.* **380,** 229–232.
8. Anderson, J. A., Huprikar, S. S., Kochian, L. V., Lucas, W. J. & Gaber, R. F. (1992) *Proc. Natl. Acad. Sci. USA* **89,** 3736–3740.
9. Sentenac, H., Bonneaud, N., Minet, M., Lacroute, F., Salmon, J. M., Gaymard, F. & Grignon, C. (1992) *Science* **256,** 663–665.
10. Christie, M. J. (1995) *Clin. Exp. Pharmacol. Physiol.* **22,** 944–951.
11. Sigworth, F. J. (1993) *Q. Rev. Biophys.* **27,** 1–40.
12. Liman, E. R., Hess, P., Weaver, F. & Koren, G. (1991) *Nature (London)* **353,** 752–756.
13. Hoshi, T., Zagotta, W. N. & Aldrich, R. W. (1990) *Science* **250,** 533–538.
14. Aldrich, R. W. (1994) *Curr. Biol.* **4,** 839–840.
15. Rettig, J., Heinemann, S. H., Wunder, F., Lorra, C., Parcej, D. N., Dolly, J. O. & Pongs, O. (1994) *Nature (London)* **369,** 289–294.
16. Li, M., Jan, Y. N. & Jan, L. Y. (1992) *Science* **257,** 1225–1230.
17. Wei, A., Solaro, C., Lingle, C. & Salkoff, L. (1994) *Neuron* **13,** 671–681.
18. Kramer, R. H., Goulding, E. & Siegelbaum, S. A. (1994) *Neuron* **12,** 655–662.
19. Pearson, R. B. & Kemp, B. E. (1991) *Methods Enzymol.* **200,** 62–81.
20. Kumar, V. D. & Weber, I. T. (1992) *Biochemistry* **31,** 4643–4649.
21. Cao, Y., Ward, J. M., Kelly, W. B., Ichida, A. M., Gaber, R. F., Anderson, J. A., Uozumi, N., Schroeder, J. I. & Crawford, N. M. (1995) *Plant Physiol.* **109,** 1093–1106.
22. Noble, M., Lewis, S. A. & Cowan, N. J. (1989) *J. Cell Biol.* **109,** 3367–3376.
23. Avdonin, V., Shibata, E. F. & Hoshi, T. (1997) *J. Gen. Physiol.* **109,** 169–180.
24. Wilson, L. and Jordan (1994) in *Microtubules*, eds. Hyams, J. S. & Lloyd, C. W. (Wiley–Liss, New York), pp. 59–83.
25. Spector, P. S., Curran, M. E., Zou, A. R., Keating, M. T. & Sanguinetti, M. C. (1996) *J. Gen. Physiol.* **107,** 611–619.
26. Miller, A. G. & Aldrich, R. W. (1996) *Neuron* **16,** 853–858.
27. Schliwa, M. (1982) *J. Cell Biol.* **92,** 79–91.
28. Tzounopoulos, T., Maylie, J. & Adelman, J. P. (1995) *Biophys. J.* **69,** 904–908.
29. Almers, W. (1978) *Rev. Physiol. Biochem. Pharmacol.* **82,** 96–190.
30. Dryja, T. P., Finn, J. T., Peng, Y. W., McGee, T. L., Berson, E. L. & Yau, K. W. (1995) *Proc. Natl. Acad. Sci.* **92,** 10177–10181.
31. Hopkins, W. F., Demas, V. & Tempel, B. L. (1994) *J. Neurosci.* **14,** 1385–1393.
32. Larsson, H. P., Baker, O. S., Dhillon, D. S. & Isacoff, E. Y. (1996) *Neuron* **16,** 387–397.
33. Papazian, D. M., Shao, X. M., Seoh, S. A., Mock, A. F., Huang, Y. & Wainstock, D. H. (1995) *Neuron* **14,** 1293–1301.
34. Schönherr, R. & Heinemann, S. H. (1996) *J. Physiol. (London)* **493,** 635–642.
35. Goulding, E. H., Tibbs, G. R. & Siegelbaum, S. A. (1994) *Nature (London)* **372,** 369–374.